Chapter 20
Specifications and Results of Centrifuge Model Test at Zhejiang University for LEAP-UCD-2017

Kai Liu, Yan-Guo Zhou, Yu She, Di Meng, Peng Xia, Jin-Shu Huang, Gang Yao, and Yun-Min Chen

Abstract Three dynamic centrifuge tests with different densities (corresponding to loose, medium dense, and dense deposits) were conducted at Zhejiang University for LEAP-UCD-2017 for an exercise of repeatability and reproducibility. The same model used in LEAP-GWU-2015 representing a 5-degree slope consisting of saturated Ottawa F-65 was repeated in 2017, but more rigorous protocols and new techniques (CPT and high-speed cameras) were included in Zhejiang University experiments. Test facilities and detailed modeling and testing procedures are presented; uncertainties in input parameters are also discussed. Preliminary results associated with selected experiment are presented.

20.1 Introduction

LEAP is an international collaboration aiming to establish rigorous protocols for validation of soil liquefaction numerical models for practical applications (Kutter et al. 2015; Manzari et al. 2015). LEAP has several exercises focusing on different aspects of liquefaction (Carey et al. 2017). In LEAP-Kyoto-2013 and LEAP-Kyoto-2014, some inconsistencies at different centrifuge facilities were noted due to laminar containers, which also caused challenges for numerical simulations (Tobita et al. 2015). Thus in LEAP-GWU-2015, a simple boundary condition (rigid container) and other specifications were proposed for more consistent results, and an identical 5-degree sloping deposit with medium dense Ottawa F-65 sand was repeated at six centrifuge facilities, and several predictors conducted numerical simulations for validation exercises. Kutter et al. (2017) compared the experimental results and found larger differences than ideal due to variability of input parameters

K. Liu · Y. She · D. Meng · P. Xia · J.-S. Huang · G. Yao
Institute of Geotechnical Engineering, Zhejiang University, Hangzhou, China

Y.-G. Zhou (✉) · Y.-M. Chen
Department of Civil Engineering, Zhejiang University, Hangzhou, China
e-mail: qzking@zju.edu.cn

B. Kutter et al. (eds.), *Model Tests and Numerical Simulations of Liquefaction and Lateral Spreading*, https://doi.org/10.1007/978-3-030-22818-7_20

(i.e., density, fabric, saturation, etc.) at different facilities. The Kyoto and GWU exercises promoted development of understanding in mechanism and protocols of specifications for later LEAP exercises. Several numerical simulations showed great consistencies with experimental tests, providing a good opportunity for uncertainty and sensitivities analysis. For the purpose of repeatability and reproducibility, better practical experimental technology and measuring techniques were adopted in LEAP-UCD-2017 for uncertainty quantification and quality control, including CPT tests for density estimation, high-speed camera for tracing surface lateral displacement, and shear-wave velocity for detecting initial state of the model (Zhou et al. 2017); other techniques like pressure sensors in RPI (Kokkali et al. 2017) were also encouraged to use for an abundant dataset.

Besides large geotechnical centrifuge ZJU-400, uniaxial hydraulic shaker, and advanced in-flight bender element (BE) system, other unique techniques, including a two-dimensional in-flight miniature CPT system and high-speed camera, were also used in Zhejiang University in LEAP-UCD-2017. Zhejiang University rigorously followed the specifications and procedures and conducted three important models with different densities, corresponding to loose, medium dense, and dense deposits. This paper describes the detailed facilities and test procedures; uncertainty analysis in input parameters and some preliminary experimental results are discussed as well, which is expected to help further researchers to understand the experimental benchmark data of Zhejiang University in LEAP-UCD-2017.

20.2 Test Facilities and Specifications

20.2.1 Test Facilities

The LEAP-UCD-2017 tests of Zhejiang University were conducted using the ZJU-400 centrifuge with in-flight uniaxial shaker and BE testing system, which was described in detail in Zhou et al. (2017).

Significant uncertainty in soil density among six facilities in LEAP-GWU-2015 has been recognized, so standard cone penetration tests were specified in LEAP-UCD-2017, including identical procedure and cone with specified diameter, tip material, and penetration rate but different length with respect to container's size. A two-dimensional (i.e., moving horizontally and penetrating vertically) miniature CPT actuation system was developed for in-flight measurement of centrifuge model ground at Zhejiang University. The CPT system shown in Fig. 20.1 includes the cone, guiding frame, and driving apparatus. CPT tests have been conducted before each destructive motion to evaluate the uniformity and density of the soil model, and the velocity of penetration was 0.6 mm per second and sample rate was 1 Hz.

The inner dimensions of the rigid model container (Fig. 20.2) are 770 mm long, 400 mm wide, and 500 mm deep. The end walls are made of 2-cm-thick iron plates with pterygoid laminas weld around the outer wall at different levels to ensure high strength and stiffness in order to avoid little distortion during shaking.

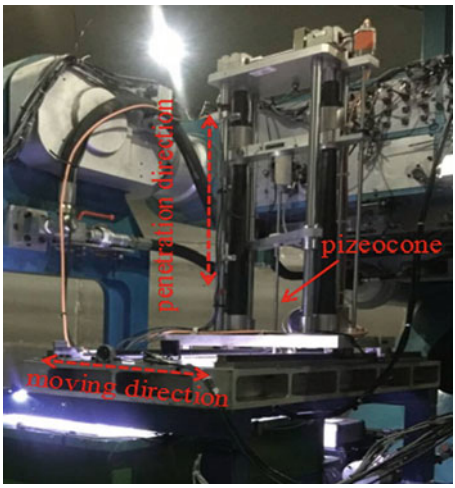

Fig. 20.1 In-flight miniature CPTu system

Fig. 20.2 Rigid container

20.2.2 Container Modifications and High-Speed Camera Installation

The container was shortened to 666 mm in length to match the prototype specification of 20 m in length with g-level of 30 and to provide room for supporting block for supporting the thick rigid plastic cover. The supporting blocks are 52-mm-thick aluminum plate, which is braced at six locations and bolted to the end walls of the container. The block was sealed to prevent drainage along the aluminum-container interfaces.

Five high-speed cameras with good resolution were used to record the lateral displacement of surface markers on different regions of the model during spinning. A partially submersed thick rigid plastic bolted with the supporting blocks at opposite ends of the container was used to prevent surface wave of liquid.

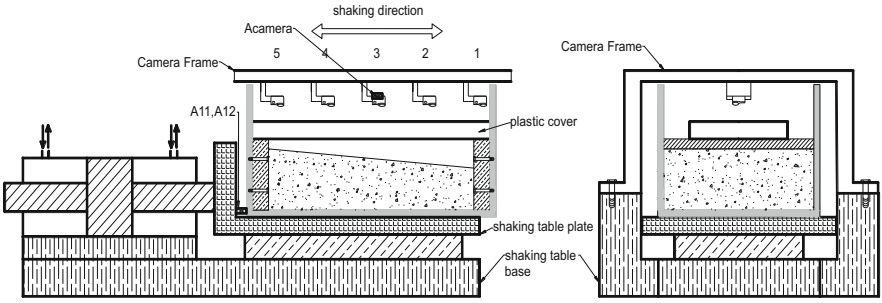

Fig. 20.3 Structure with cameras and supporting block installation

The structure with cameras is as shown in Fig. 20.3. The cameras embraced with aluminum frame were bolted with camera frame, which is also bolted with shaking table base. The movement between the camera frame and the container bolted with shaking table plate is the same during shaking. The displacement obtained from video includes three components: movement of camera frame (d1), the container (d2), and the surface marks relative to the container (d3), above which the last component is of interest. Acceleration records of the accelerometer (A_{camera}) installed at the middle camera and A11 (A12) were used to obtain movement of camera frame and the container, respectively, by double integration.

20.2.3 Model Description

The same model used in LEAP-GWU-2015 was repeated in LEAP-UCD-2017. The model represents a 5-degree, 4-m-depth at midpoint, 20-m-length sand slope deposit of Ottawa F-65. It notes that the shaking direction is parallel to the axis of the centrifuge. The soil surface normal to slope direction was not curved according to the radius of the centrifuge. Considering the centrifuge radius to surface of the model and width of container are 4182 mm and 400 mm, respectively, the flat surface in the end view represented a gentle 0.14-m-high, 12-m-wide hill in prototype scale, with an average ground slope of 2.4% toward the side walls of the container.

The instruments are shown in Fig. 20.4. The required and highly recommended sensors were installed in the model. There were six accelerometers AH1 to AH9 inside the model recording horizontal acceleration and the other four (AH11, AH12, AV1, and AV2) on the container to monitor the input motion in both horizontal and vertical direction. Eight pore pressure transducers of P1 to P10 were also installed inside the model. Three pairs of bender elements, at the same depth with pore pressure transducers (elements S1-R1, S2-R2, and S3-R3 were located at the same

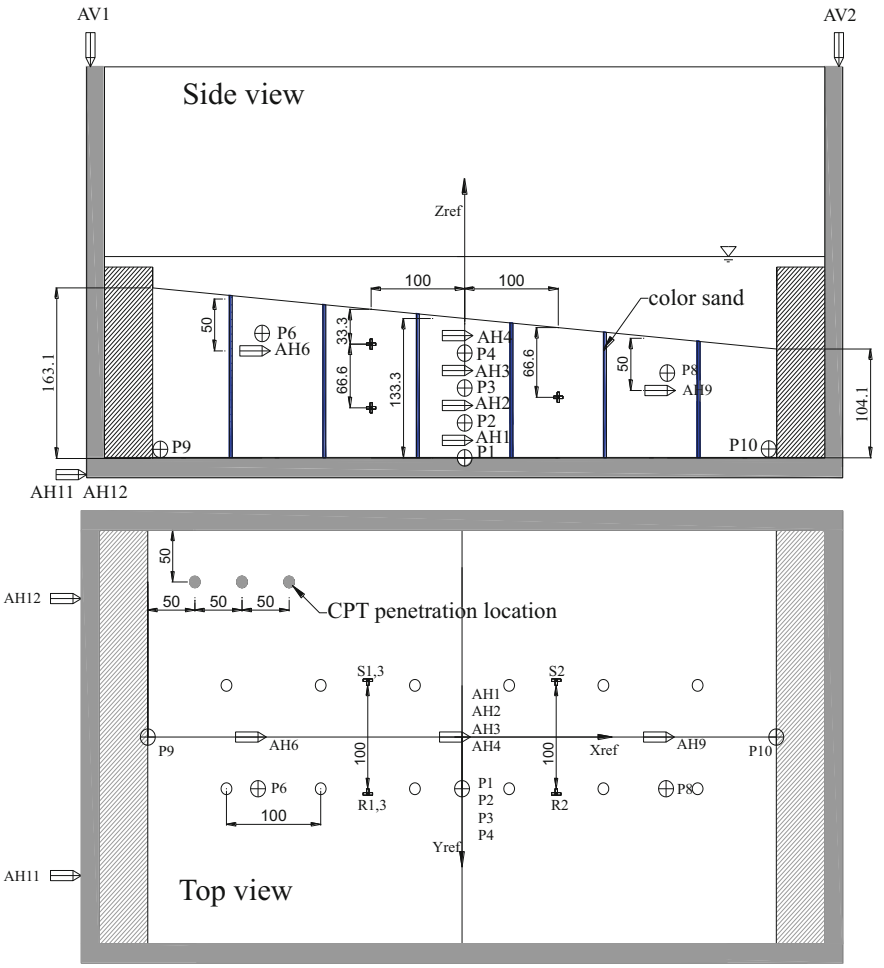

Fig. 20.4 Centrifuge model setup and installation locations

depth as P4, P3, and P2, respectively), were placed to measure vertically polarized and horizontal travelling SV shear-wave velocity.

Surface markers were used to trace surface displacement. The specified surface markers are shown in Fig. 20.5 in red, which consists of a 10-mm-length, 25-mm-in-diameter PVC tube with an aluminum cross bar fixed in center. In addition, surface markers made of zip ties were also used, and all the surface markers were installed in a 0.05 m $\times$ 0.05 m grid (model scale). Colored sand columns following the same method as described in Zhou et al. (2017) were used to determine lateral spread profiles by excavation after finally spin-down.

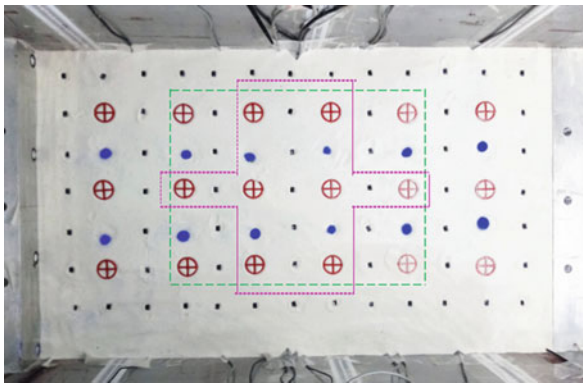

Fig. 20.5 Surface markers and colored sand columns

Table 20.1 Properties of Ottawa sand used in ZJU for each model

Model	Target density (kg/m^3)	Achieved density (kg/m^3)	Min. density (kg/m^3)	Max. density (kg/m^3)	D10 (mm)	D30 (mm)	D60 (mm)
ZJU1	1651	1672	1496	1784	0.116	0.148	0.186
ZJU2	1599	1606	1491	1786	0.102	0.136	0.186
ZJU3	1703	1706	1490	1786	0.104	0.137	0.186

20.3 Centrifuge Experiment Preparation

20.3.1 Properties of Test Material

For eliminating the effect of inconsistency of Ottawa F-65 at different facilities on model response, maximum and minimum dry density and grain analysis tests were conducted before each model according to "Chinese code for soil tests for hydropower and water conservancy engineering, 2006," and the results are summarized on Table 20.1. Figure 20.6 shows the grain-size distribution curve for three models, and there are little differences in grain-size distribution among three models. Additional material properties are available in Carey et al. (2016). In LEAP-UCD-2017 the density was specified instead of void ratio, and the target and achieved densities for ZJU1, ZJU2, and ZJU3 are summarized in Table 20.1 and correspond to loose, medium dense, and dense model.

20.3.2 Achieved Density

Air pluviation method was adopted to ensure a high level of uniformity. The apparatus for air pluviation and construction procedures are available in Zhou et al. (2017). The calibration results using the specified spout were different from

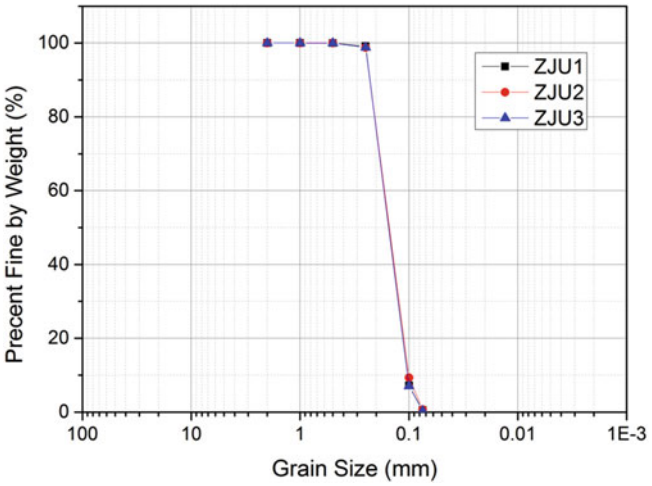

Fig. 20.6 Grain-size distribution curve

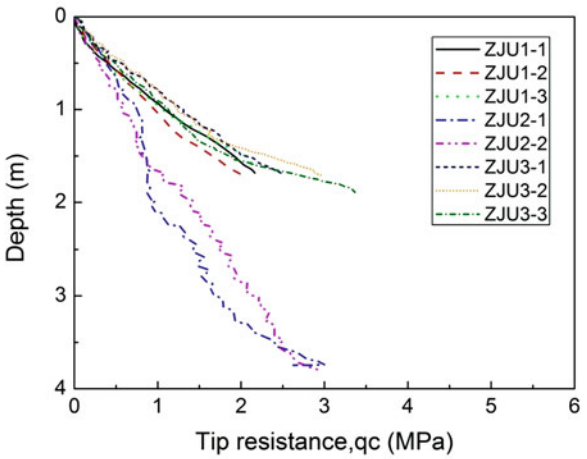

Fig. 20.7 Cone tip resistance profile results

that specified. So a spout with one slot shape was adopted. ZJU1 and ZJU2 adopted the same calibration curve, which could not meet the specified density of ZJU3, so that a spout with a thinner slot was used. There was 3–4 kg/m^3 difference between two calibration results at the same drop height, besides the falling height changed less than 2 cm during pluviation, which causes a maximum deviation of 7 and 8 kg/cm^3 from the target density for ZJU1 (ZJU2) and ZJU3, respectively. Moreover the model settled after saturation. Overall, the achieved density is expected to deviate from the target within $\pm$11 kg/m^3.

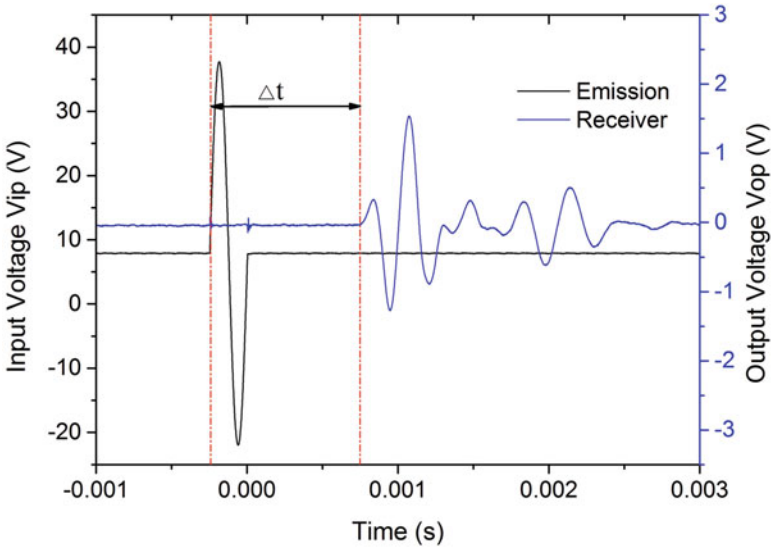

Fig. 20.8 Typical signals of In-flight BE

20.3.3 Saturation

Silicone oil (RC0201-30cST, $\rho_d = 955$ kg/m^3 at 25 °C) with 30 times of viscosity of water was used as pore fluid to satisfy the scaling law. The oil tank and model container were kept under the same vacuum level and the oil was de-aired, and the transport from the reservoir to the container was driven by gravity feed. The saturation speed was controlled to prevent soil disturbance at the bottom of container. The degree of saturation for three models was not measured; however, the saturation devices and procedures were the same with these used in LEAP-GWU-2015, which provides a reference of degree of saturation for three models, indicating achieved $S_r > 99.5\%$.

20.4 Test Procedure and Achieved Motions

20.4.1 Test Procedure

The test procedure is shown in Table 20.2. A careful survey of the surface markers was made before spin-up. Then the centrifuge was spun up to 10 g, 20 g, and 30 g step by step. The V_s was measured on each g-level when the pore pressure at this stage was stable. After consolidation in 30 g, the model was subjected to step-wave motion, which was too small to generate any excess pore pressure and was used to

Table 20.2 Test procedure and events of interest in the test

No.	Name	N(g)	Description	No.	Name	N(g)	Description
1	S-1	1	Surface marker survey	18	CPT-2	30	CPT test
2	A		Swing-up	19	E	30	Motion2
3	BE-1	10	V_s measurement	20	BE-8	30	V_s measurement
4	BE-2	20	V_s measurement	21	SW-4	30	Step wave
5	BE-3	30	V_s measurement	22	F		Start of swing-down
6	SW-1	30	Step wave	23	S-3	1	Surface marker survey
7	CPT-1	30	CPT test	24	G		Start of swing-up
8	B	30	Motion1	25	BE-9	10	V_s measurement
9	BE-4	30	V_s measurement	26	BE-10	20	V_s measurement
10	SW-2	30	Step wave	27	BE-11	30	V_s measurement
11	C		Start of swing-down	28	SW-5	30	Step wave
12	S-2	1	Surface marker survey	29	CPT-3	30	CPT test
13	D		Start of swing-up	30	H	30	Motion3
14	BE-5	10	V_s measurement	31	BE-12	30	V_s measurement
15	BE-6	20	V_s measurement	32	SW-6	30	Step wave
16	BE-7	30	V_s measurement	33	I		Start of swing-down
17	SW-3	30	Step wave	34	S-4	1	Surface marker survey

characterize the model. Then CPT test was conducted for determining the density of the model and then motion1 (destructive motion) followed. Enough time was needed for full dissipation of excess pore pressure in the soil, then step wave was used again to characterize the deposit, and the centrifuge was spun down and surface markers were surveyed. Thereafter the centrifuge spun up and later procedures were the same as before except for destructive motions. V_s was measured by bender elements before and after each destructive motion when the pore pressure was stable at each stage. Three models followed the same procedures.

20.4.2 In-Flight Characterizations

Figure 20.7 shows the cone tip resistance results versus depth profile for three models. Because of design mistakes of CPT support device above the container, the penetration depths for ZJU1 and ZJU3 are less than 2 m in prototype scale. Unfortunately, due to time constraints associated with LEAP program, the deficient CPT support device was adopted in ZJU1 and ZJU3, the improved device was used in ZJU2, and the penetration depth was up to 4 m in prototype scale.

The bender elements (BE) used in tests are electrically shielded and grounded to avoid undesired electromagnetic interfere in centrifuge environment. Shown in Fig. 20.8 is a typical signal of BE during spinning, indicating the arrival of receiver is well distinguishable to ensure reliable results of BE. The V_s data and associated analysis will be presented in a later publication.

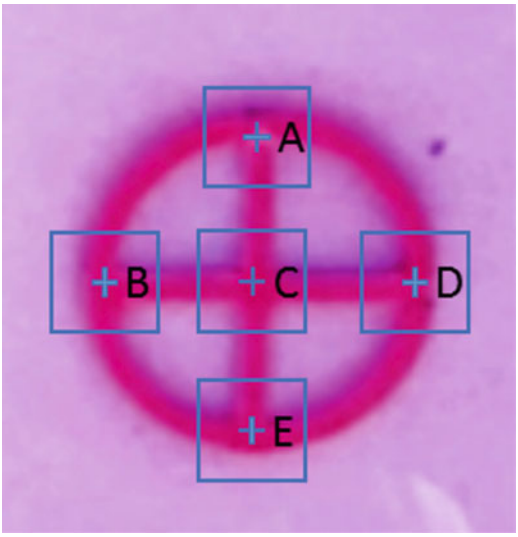

Fig. 20.9 PIV analysis points of surface marker

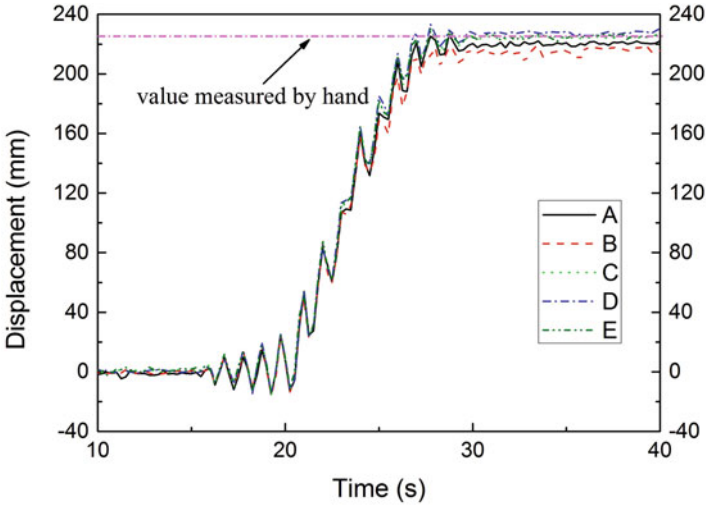

Fig. 20.10 Typical results from PIV analysis

As mentioned above, five GoPro cameras were installed above the slope surface to record movement of surface markers. The videos were converted to displacement time history by GeoPIV analysis procedure. There are five points located at different regions of the surface marker used to ensure reliable results shown in Fig. 20.8. Figure 20.10 shows typical results of dynamic displacement of one surface marker from five points, showing high consistency within five points. And also, the displacement value obtained using videos is consistent with that measured by hand afterward.

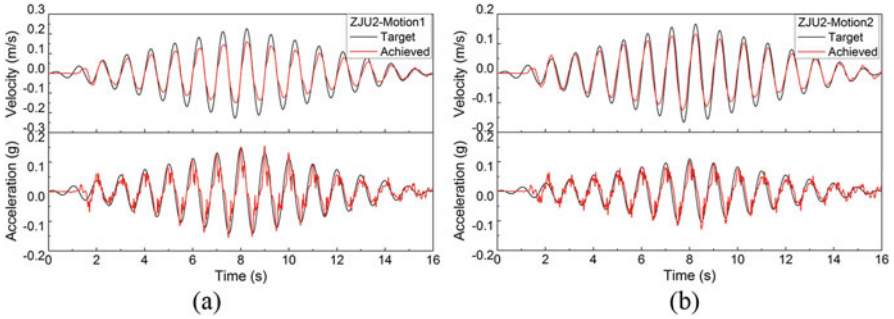

Fig. 20.11 Achieved and specified acceleration and velocity time history: (**a**) ZJU2-motion1; (**b**) ZJU2-motion2

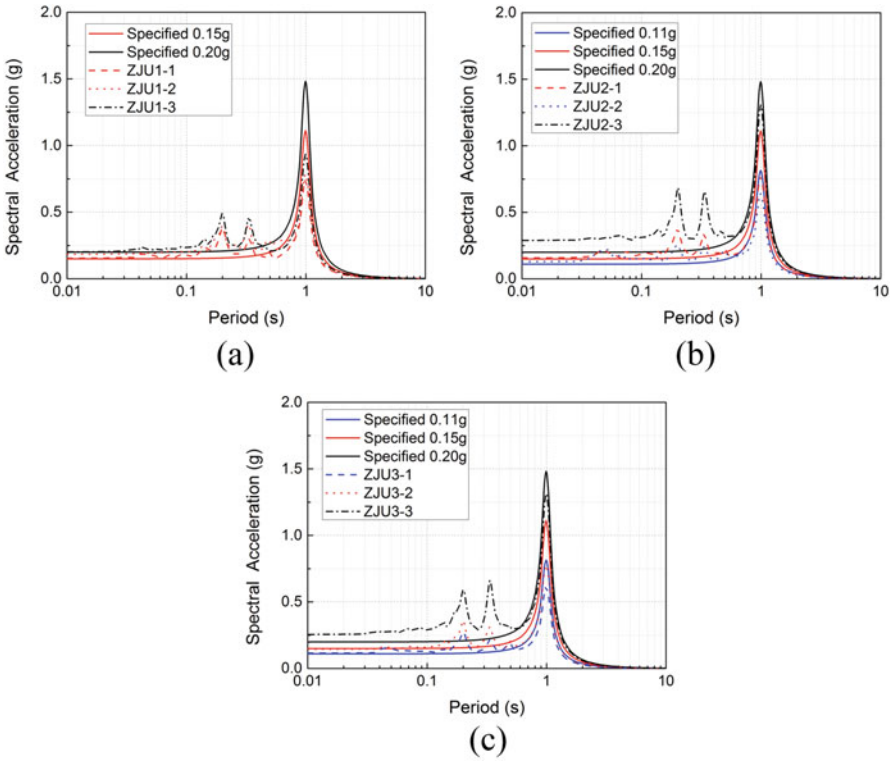

Fig. 20.12 Achieved and specified 5% damped acceleration response spectra: (**a**) ZJU1; (**b**) ZJU2; (**c**) ZJU3

20.4.3 Achieved Horizontal Components

For length limitation, only selected achieved horizontal base accelerations are presented in Fig. 20.11 and compared with target accelerations. The shown

Table 20.3 Ground motion sequence for LEAP-UCD-2017 experiments, unit:g

Model	Motion	Target PGA_{eff}	A11			A12		
			PGA_{1Hz}	PGA_{hf}	PGA_{eff}	PGA_{1Hz}	PGA_{hf}	PGA_{eff}
ZJU1	Motion111	0.15	0.093	0.070	0.128	0.093	0.071	0.128
	Motion2	0.15	0.099	0.093	0.146	0.100	0.093	0.147
	Motion3	0.20	0.118	0.101	0.169	0.118	0.095	0.166
ZJU2	Motion1	0.15	0.097	0.083	0.139	0.098	0.088	0.142
	Motion2	0.11	0.079	0.061	0.110	0.08	0.066	0.113
	Motion3	0.2	0.164	0.126	0.227	0.164	0.127	0.228
ZJU3	Motion1	0.11	0.077	0.051	0.103	0.077	0.045	0.100
	Motion2	0.15	0.097	0.073	0.134	0.098	0.072	0.134
	Motion3	0.2	0.164	0.101	0.215	0.165	0.097	0.214

acceleration time histories are filtered with a 0.2 Hz (prototype scale) high-pass filter, and the achieved acceleration matches the specified motion well. In LEAP-2017, a new concept of effective PGA was adopted to evaluate the accuracy and efficiency of the motions. The effective PGA is defined as below:

$$PGA_{effective} = PGA_{1Hz} + 0.5 \times PGA_{hf} \tag{20.1}$$

where PGA_{hf} represents the peak acceleration of the high-frequency component of the motion and PGA_{1Hz} denotes the peak acceleration with bandpass filtering of 0.9–1.1 Hz. The results of all the input motions for three models are summarized in Table 20.3. It is found that PGA_{1Hz} values are almost the same between AH11 and AH12 for one input motion, indicating the inputs of shaking table plane are uniform.

The results showed that it is not easy to make the achieved motions match well with the target because the high-frequency components vary so abruptly and arbitrarily. However, the experiences learned from ZJU1 are important to accurately control the further base motions of ZJU2 and ZJU3. The achieved motions matched well with the target in amplitude and waveform, and the three models provide good benchmarks for numerical predictors.

Five percent damped acceleration response spectra (ARS) for all motions for three models are shown in Fig. 20.12. All achieved peak spectral accelerations were smaller than the specified at the main intended frequency of 1 Hz and showed high-frequency components. The achieved peak acceleration in 1 Hz (prototype scale) was almost identical for motions with the same target peak acceleration, which shows a good performance of the hydraulic shaker.

20.4.4 Achieved Vertical Components

Figure 20.13 displays the selected vertical accelerations measured by AV1 and AV2 at opposite ends of container. Although zero vertical acceleration is desired during shaking, the hydraulic shaker produced unintended vertical component in

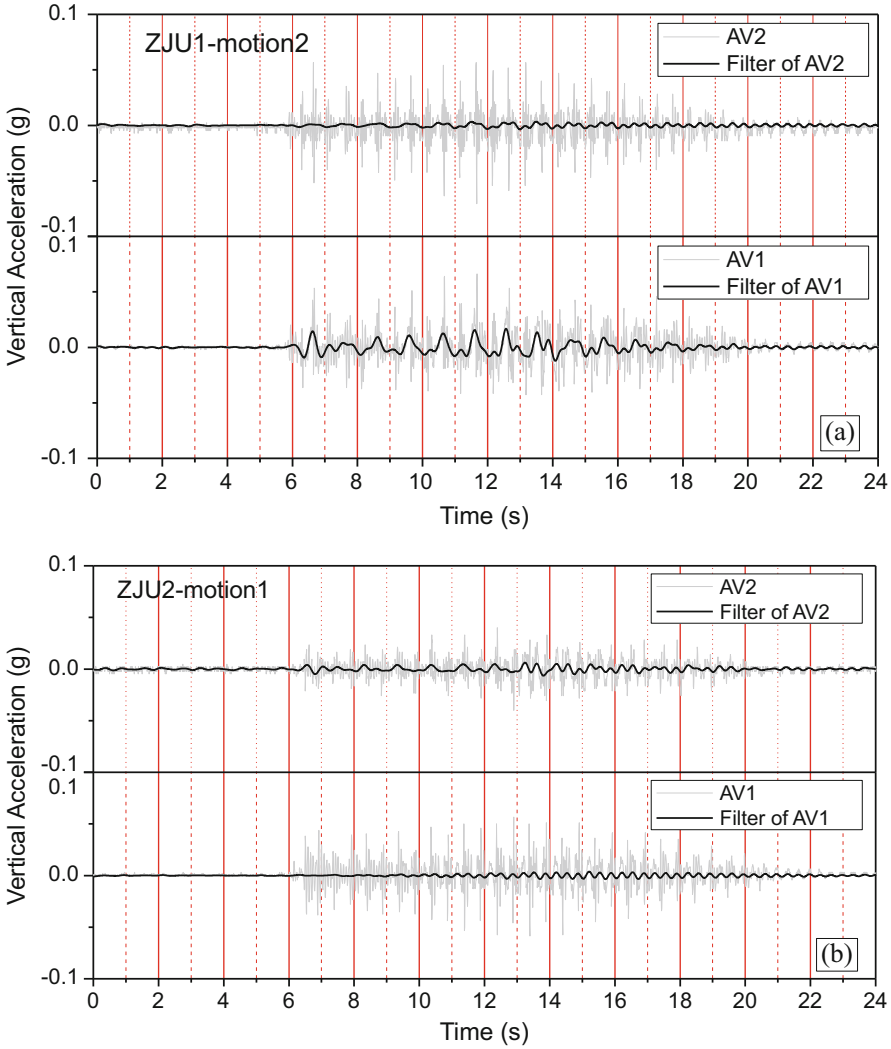

Fig. 20.13 Vertical accelerations on container ends: (**a**) ZJU1-motion2; (**b**) ZJU2-motion1

addition to the horizontal accelerations. The gray lines indicate unfiltered vertical motions, and the black ones, bandpass filtering with 0.3–3 Hz in consistency with Kutter et al. (2017) to reduce high frequency noise, are superimposed as well. The amplitude of the filtered vertical component ranges from 4% to 17% of the achieved 1 Hz horizontal component. The rocking accelerations are not very large and the larger spikes are of relatively high frequency. It is worth noting that the angular displacement due to rocking is very small as shown in Fig. 20.14 for ZJU1-motion2

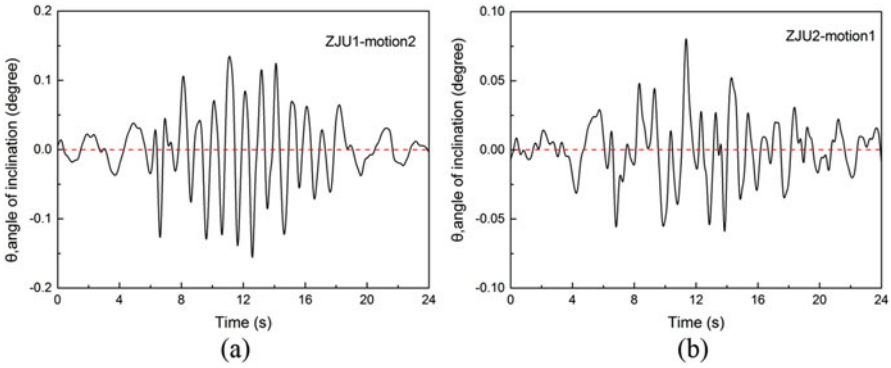

Fig. 20.14 Angle of rocking displacement during shaking: (**a**) ZJU1-motion2; (**b**) ZJU2-motion1

and ZJU2-motion1, respectively. The angle of inclination was computed by integrating accelerations to obtain vertical displacements of AV1 and AV2. The difference in these displacements was divided by the length of the box to determine the rocking angle shown in Fig. 20.14. The maximum rocking angle during shaking was no more than 0.15 degrees along longitudinal direction of the container, indicating rocking displacements can be neglected during shaking.

20.5 Results

20.5.1 Acceleration Responses

Figures 20.15 and 20.16 only show the acceleration time histories and Fourier spectrum of motion1 and motion3 in ZJU3 because of length restriction. For motion1 in ZJU3, the trace of accelerations recorded at base and central array along the depths is very similar during shaking, and obvious amplification effect was observed, indicating the soil moves almost as a rigid mass and the shear strain accumulated in the soil is small; however, for motion3 in ZJU3, the acceleration time history shows de-amplification in upslope direction and negative spikes in downslope direction, which was observed in LEAP-GWU-2015 and other previous studies (Zeghal and Elgamal 2015). Looking closely at the excess pore pressure time history during motion1 and motion3, there was little liquefaction occurring during motion1 and severe liquefaction happening during motion3, which accounts for different site responses of acceleration. It finds that the spikes mainly consist of high-frequency components when comparing Fourier spectrum of motion1 and motion3.

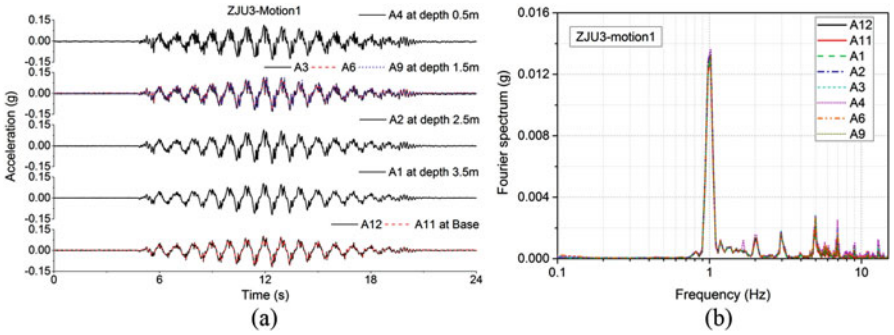

Fig. 20.15 ZJU3-motion1: (**a**) acceleration time history; (**b**) Fourier spectrum

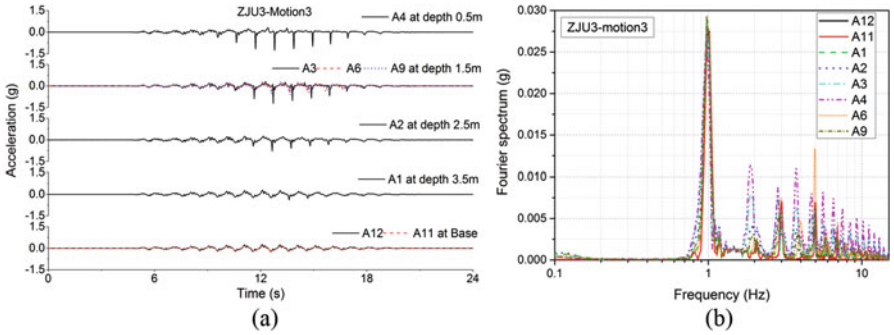

Fig. 20.16 ZJU3-motion3: (**a**) acceleration time history; (**b**) Fourier spectrum

20.5.2 Pore Pressure Response

Figure 20.17 shows the time history of excess pore pressure ratio for motion1 and motion3 in ZJU3. It notes that pore pressure sensors of P1 and P9 didn't work well due to without full saturation disposure before being placed in model, the same problem with P1 and P3 in ZJU1. For motion1 in ZJU3, excess pore pressure generated rapidly and started dissipating before the end of shaking; no liquefaction occurred even in shallow depth. However, severe liquefaction happened during motion3 in ZJU3; significant sudden drops in excess pore pressure due to dilatancy were observed, which corresponds to large spikes in acceleration. Figure 20.17 clearly depicts liquefaction state arose at shallow depth and then propagated downward. After maintaining for a while, then dissipation began after the end of shaking. The dissipation of excess pore pressure started early at deep depth, and then solidification front (red circle) moved upward.

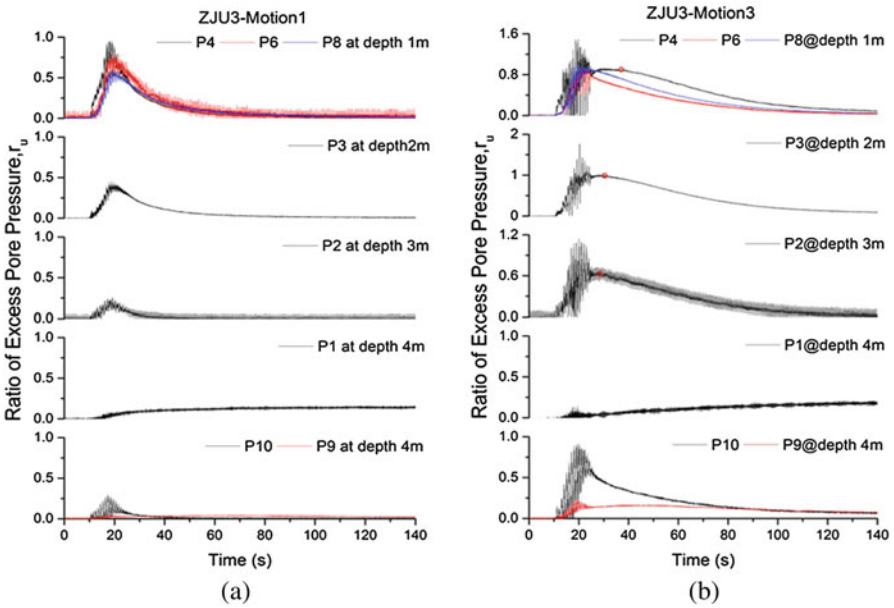

Fig. 20.17 Pore pressure time history: (**a**) ZJU3-motion1; (**b**) ZJU3-motion3

20.5.3 Displacement Response

Vertical Displacement D_v Response

The vertical displacements (D_v) were surveyed via the specified red surface markers after each motion, and the average values and standard deviation of vertical displacement for each motion calculated from only red surface in pink dashed frame shown in Fig. 20.5 are summarized in Table 20.4 in prototype scale. The standard deviations of D_v of the surface markers are less than 20%, indicating the discreteness of the data is relatively small.

Horizontal Displacement D_v Response

Average values and standard deviation of lateral displacement (D_L) of surface markers in green dashed frame shown in Fig. 20.5 after each motion are summarized in Table 20.5 in prototype scale. The standard deviations of D_v for the surface markers are within 63%, indicating it is acceptable that the average value represents the overall level of lateral displacement.

Figure 20.18 shows the lateral displacement profiles from excavation. The profiles showed that the displacement distributed over the whole depth and reached the maximum at the surface.

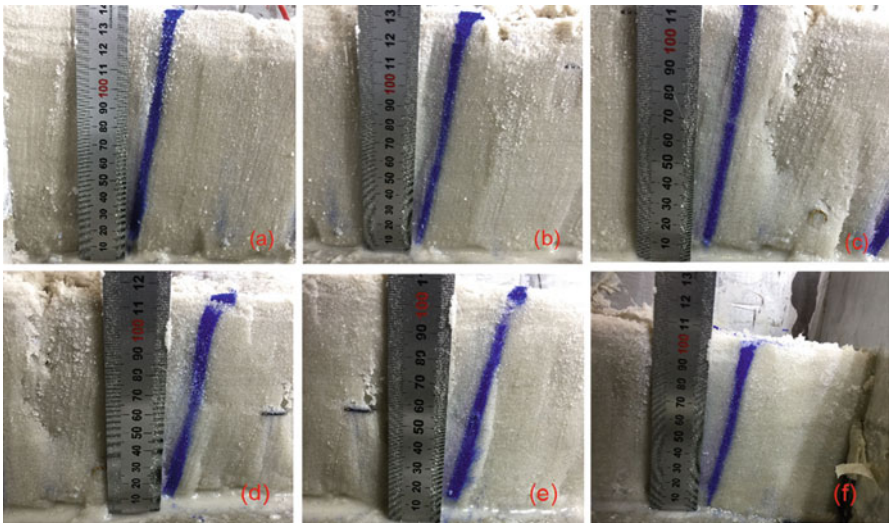

Fig. 20.18 Typical lateral displacement profiles from excavation for ZJU2 model: pictures from (**a**) to (**e**) correspond to six colored sand columns from the top to the toe

Table 20.4 Average vertical displacements after each motion

	Motion1		Motion2		Motion3	
Model	μ^a/mm	σ^b	μ/mm	σ	μ/mm	σ
ZJU1	42.4	13	30.0	16	24.0	5
ZJU2	57.4	20	13.9	5	21.4	20
ZJU3	22.9	10	7.9	7	39.0	14

[a]Average value
[b]Standard deviation of vertical displacement of the 12 red surface markers in green dashed frame shown in Fig. 20.5

Table 20.5 Average values of lateral displacement after each motion

	Motion1		Motion2		Motion3	
Model	μ^a/mm	σ^b	μ/mm	σ	μ/mm	σ
ZJU1	151	51	55	63	36	28
ZJU2	293	35	38	22	200	18
ZJU3	22.9	10	7.9	7	39.0	14

[a]Average value and
[b]Standard deviation of horizontal displacement of surface markers in green dashed frame shown in Fig. 20.5

20.6 Summary and Conclusions

Three important centrifuge tests were conducted at Zhejiang University in LEAP-UCD-2017. Three models were designed in different densities corresponding to loose, medium dense, and dense Ottawa sand deposit for a comprehensive comparison of density effect on site response. The main purpose of this paper is to help further researcher to understand the data of tests uploaded in NEES website, so that information on test facilities, model setup and preparation, test procedures, and analysis of the results is presented.

Besides the centrifuge, shaking table, and in-flight BE system used in LEAP-GWU-2015, a two-dimensional miniature CPTu system was used to determine the density of the deposit following the specified and identical procedures and cone. High-speed cameras were installed above the model to trace the displacement of surface markers; the structures with cameras and the method to obtain displacement time history are introduced. The model preparation and tests procedures are also detailed. The pluviation devices and procedures lead to uncertainty in density within ± 11 kg/m^3 with the achieved density. The degree of saturation for three models was not measured but based upon previous experience with this method (Zhou et al. 2017), the achieved $S_r > 99.5\%$.

The base input acceleration closely matched the target, but velocity was slightly smaller. The achieved effective PGA for each motion roughly match the targets. Five percent damped acceleration response spectra show the achieved motions were smaller than the target of 1 Hz components and some high-frequency components in input motion. The vertical accelerations at opposite ends of container were small, indicating a negligible rocking effect during shaking.

Results of motion1 and motion3 for ZJU3 are exampled to illustrate different responses to liquefaction and non-liquefaction. Motion1 didn't trigger liquefaction even at shallow depth but high excess pore pressure generating during shaking, the trace of accelerations for the base motion and central array is very similar, and an obvious amplification in amplitude was observed; there were no spikes for motion1. Motion3 led to severe liquefaction up to 2 m below the surface; spikes in acceleration time history due to dilatancy are consistent with drops in excess pore pressure. Lateral and vertical displacements for each motion were surveyed via some surface markers. Low standard deviation indicates high confidence with results.

Acknowledgments This study is partly supported by the National Natural Science Foundation of China (Nos. 51578501, 51778573), the National Program for Special Support of Top-Notch Young Professionals (2013), the Zhejiang Provincial Natural Science Foundation of China (No. LR15E080001), and the National Basic Research Program of China (973 Project) (No. 2014CB047005).

References

Carey, T. J., Hashimoto, T., Cimini, D., & Kutter, B. L. (2017). LEAP-GWU-2015 centrifuge test at UC Davis. *International Journal of Soil Dynamics and Earthquake Engineering, 113*, 663–670. https://doi.org/10.1016/j.soildyn.2017.01.030.

Carey, T. J., Kutter, B. L., Manzari, M. T., Zeghal, M., & Vasko, A. (2016). *LEAP soil properties and element test data*. https://doi.org/10.17603/DS2WC7W.

Kokkali, P., Abdoun, T., & Zeghal, M. (2017). Physical modeling of soil liquefaction: Overview of LEAP production test 1 at Rensselaer Polytechnic Institute. *Soil Dynamics and Earthquake Engineering*. https://doi.org/10.1016/j.soildyn.2017.01.036.

Kutter, B. L., Manzari, M. T., Zeghal, M., Zhou, Y. G., & Armstrong, R. J. (2015). Proposed outline for LEAP verification and validation processes. In S. Iai (Ed.), *Geotechnics for catastrophic flooding events* (p. 99–108). London: Taylor & Francis.

Kutter B. L., Carey T. J., Hashimoto T., Zeghal M., Abdoun T., Kokkali P., Madabhushi G., Haigh S., d'Arezzo F. B., Madabhushi S., Hung W. Y., Lee C. J., Cheng H. C., Iai S., Tobita T., Ashino T., Ren J. F., Zhou Y. G., Chen Y. M., Sun Z. B., Manzari M. T. (2017). LEAP-GWU-2015 experiment specifications, results, and comparisons. *International Journal of Soil Dynamics and Earthquake Engineering, 113*, 618–28.

Manzari, M. T., Kutter, B. L., Zeghal, M., Iai, S., Tobita, T., Madabhushi, S. P. G., Haigh, S. K., Mejia, L., Gutierrez, D. A., & Armstrong, R. J. (2015). LEAP projects: Concept and challenges. In *Proceedings of the fourth international conference on geotechnical engineering for disaster mitigation and rehabilitation (4th GEDMAR): 2014 Sept 16–18*. Kyoto: Taylor & Francis.

Tobita, T., Manzari, M. T., Ozutsumi, O., Ueda, K., Uzuoka, R., & Iai, S. (2015). Benchmark centrifuge tests and analyses of liquefaction-induced lateral spreading during earthquake. In S. Iai (Ed.), *Geotechnics for catastrophic flooding events* (p. 127–82). London: Taylor & Francis.

Zeghal, M., & Elgamal, A. Site response and vertical seismic arrays (2015). *Progress in Structural Engineering and Materials*, 2(1):92–101.

Zhou, Y.-G., Sun, Z.-B., & Chen, Y.-M. (2017). Zhejiang University benchmark centrifuge test for LEAP-GWU-2015 and liquefaction responses of a sloping ground. *International Journal of Soil Dynamics and Earthquake Engineering, 113*, 698–713. https://doi.org/10.1016/j.soildyn.2017.03.010.